

# **ASCA AND GRO OBSERVATIONS OF GX301-2**

Steven H. Pravdo<sup>1,2,3</sup>

Charles S. R. Day<sup>3,4</sup>

Lorella Angelini<sup>3,4</sup>

Alan B. Harmon<sup>5</sup>

A. Yoshida<sup>6</sup>

and

P. Saraswat<sup>6</sup>

submitted to the *Astrophysical Journal* April 1, 1995

---

<sup>1</sup>The research described in this paper was carried out in part by the Jet Propulsion Laboratory, California Institute of Technology, under contract with the National Aeronautics and Space Administration.

<sup>2</sup>Jet Propulsion Laboratory, Mail Stop 306-431, California Institute of Technology, Pasadena, CA 91109

<sup>3</sup>ASCA guest investigator

<sup>4</sup>University Space Research Association, Laboratory for High Energy Astrophysics, NASA/Goddard Space Flight Center, Code 668, Greenbelt, MD 20771

<sup>5</sup>Marshall Space Flight Center, ES84, Alabama 35812

<sup>6</sup>The Institute of Physical and Chemical Research (RIKEN), Hirosawa, 2-1, Wako-shi, Saitama35 1-01, Japan

## 1. INTRODUCTION

GX301-2 is an X-ray pulsar in a binary system with the supergiant WRA 977 (B1.5 Ia). The orbit has a period of  $41.508 \pm 0.007$  days and an eccentricity,  $e = 0.472$  (Sato et al. 1986). The X-ray spectrum has episodes of enhanced low-energy absorption (Ricker *et al.* 1973), an iron absorption edge (Swank et al. 1976), pulse-phase dependence (Leahy & Matsuoka 1990), orbital-phase dependence (Haberl 1991), and iron-line emission (Leahy et al. 1989).

The eccentric orbit results in periodic extended flares which are centered about 1.4 days before periastron passage. The flares occur when the mass accretion rate onto GX301 -2 suddenly increases. Variations in the accretion from the WRA 977 stellar wind alone do not account for the intensity variations, even considering the eccentric orbit (e.g. White and Swank 1984). Rather, following Stevens (1988), Haberl (1991) and Leahy (1991) proposed that a gas stream flowing from WRA 977 to the neutron star is the main source of accreted material. The initially puzzling result that the flares preceded periastron by 0.034 orbital phase was explained by a spiral-shaped gas stream which GX301 -2 intercepted on its approach to periastron. This model can account for the binary phase dependence of the X-ray intensity but does not explain the highest observed hydrogen column density,  $N_H$  (Haberl 1991).

The source was identified as a pulsar by White et al. (1976). Between 1973 and 1984 the pulse period behavior with time was stochastic (Nagase 1989) leading to an explanation based upon angular momentum transferred via a stellar wind (e.g. White & Swank 1984). Since 1984 a secular spin-up has occurred which, according to the theory of Ghosh & Lamb (1979), indicates that an accretion disk has formed.

This paper reports the results of an observation of GX301-2 with *ASCA* and *GRO* in the 4-60 keV range. These observations allow us to re-examine many of the previously reported results with the higher spectral resolution afforded by the *ASCA* detectors and the high energy range of *BATSE/GRO*. In addition, the spatial resolution of the *ASCA* telescope allowed us to separate GX301 -2 from the X-ray contribution of previously undetected soft X-ray sources. A related paper discusses the analysis and results of this *ASCA* observation of GX301 -2 X-ray spectrum  $\leq 4$  keV (Saraswat et al. 1995).

## 2. OBSERVATIONS

*ASCA* observed GX301-2 on 13-14 February 1994. The *ASCA* telescope and detectors are described by Tunics et al. (1994). We use both Solid-state Imaging Spectrometer (SIS) and Gas Imaging Spectrometer (GIS) data in the 0.3-10 keV range: the SIS for its superior energy resolution (about a factor of 4 compared to the GIS) and the GIS for its enhanced high-energy response ( $E > 5$  keV) and field-of-view (50 arcmin diameter).

*BATSE/GRO* provides nearly continuous coverage of GX301 -2 except for periods of Earth occultation of the source or detector shutdown (e.g. during passages of the South Atlantic Anomaly). We use intensity and spectral data in the energy range 20-60 keV obtained with occultation analysis from the Large-Area Detectors, LAD I and LAD5. These are two of the eight uncollimated NaI scintillation crystal detectors that comprise *BATSE* (Fishman et al. 1989). In particular we take *BATSE* data straddling the *ASCA* observation to construct the long-term light curve of the source, and data during the *ASCA* observation for the combined broadband spectroscopy.

### 3. RESULTS

#### 3.1 New Soft X-ray Source Near GX301-2

GX301-2 is so intense that its broadband image spills over into adjacent pixels and precludes the detection of new sources in the surrounding few arcminutes. However if we restrict the X-ray images to energies less than 2 keV we find two sources within 8'. Figure 1a shows the *GIS2* image of the sky in X-rays from 0.8-2.0 keV. Source 1 near the center of the field is GX301-2. Source 2 is located about 8' NE of GX301-2 and is a new source called AX1227-6239 (GXS). Sources 3 and 4 are weak, unidentified sources, and source 5 is probably  $\alpha$  Cru. The higher spatial resolution in the *SISO* image (Figure 1b; 0.5-2.0 keV) shows GX301-2 and another source, AX1226-6249 (SXS), which is about 3' southeast of GX301-2. This source is so weak compared to GX301-2 that it can not be resolved with the automatic analysis program. Both sources are near enough that previous observations of GX301-2 would have been contaminated in this band.

GXS is fit by a thermal spectrum with  $kT \approx 0.4$  keV. The GXS intensity based on the spectral fit is  $\sim 9 \times 10^{-13}$  erg  $\text{cm}^{-2}$   $\text{s}^{-1}$  in the 0.5-1.5 keV band. The images of GXS and GX301-2 have the same 0.5-1.5 keV band intensity to within 100%. Clearly GXS is a significant contaminant to GX301-2 in this soft band for detectors with low spatial resolution, SXS is a considerably weaker than GXS, at about 4% the GX301-2 intensity.

GXS was also detected in an *Einstein* HRI observation on August 23, 1980. At that time assuming the same spectral form, the intensity was about three times higher,  $3.5 \pm 1.5 \times 10^{-12}$  erg  $\text{cm}^{-2}$   $\text{s}^{-1}$ . A number of *EXOSAT* CMA observations in the period 1983-1985 had GXS in the field of view. Only the 20 April 1984 observation had sufficient sensitivity to detect the source although the intensity is uncertain due to the low efficiency of the Al/P filter that was used. The HRI position yielded the finding chart shown in Figure 2. GXS is identified with a  $V = 10.77$  mag star from the *Guide Star Catalog* (1989). Figure 3 shows the blue spectrum of this star. The spectral shape and prominent emission lines at Ca II H and K and H $\epsilon$  suggest that this is a dMe star (Robinson et al. 1990). Table 1 shows the equivalent widths of the detected lines.

The SXS position is known with less accuracy than GXS since we do not have a higher resolution detection elsewhere. We show in Figure 2 the position of the luminous, unidentified star MO-16 (Marraco & Orsatti 1982), which is 14" from the SXS position.

#### 3.2 GX301-2 Light Curve and Flares

Figure 4 shows the GX301-2 light curve obtained with the *BATSE* experiment in 1993-4. Seven pre-periastron flares are evident. A predicted flare centered around day 132 in the figure occurred during a gap in the data. The *ASCA* observation occurred during days 146-7 (Figure 4), GX301 orbital phase 0.27-0.29. The Haberl (1991) model for a gas stream from the primary to GX301-2 has an intensity maximum near phase 0.9 corresponding to the pre-periastron flare and a broad secondary intensity maximum near the phase of the *ASCA* observation, 0.3. This secondary maximum is not seen in the *BATSE* data (see below). The light curve of the *ASCA* data shows intensity variability by a factor of  $\sim 3$ , much of that attributable to the pulsations,

The flares are periodic and last several days. To determine the best flare period we folded the light curve data over trial periods near the GX301-2 orbital period determined by Sato et al. (1986). The highest  $\chi^2$  value for a constant model occurred for a flare period of  $41.507 \pm 0.008$  days. This period is consistent with the Sato et al. orbital and flare periods. We modeled the folded light curve

with a polynomial function and Lorentzian and/or Gaussian components. Figure 5 shows a) the folded data and b) the best-fit model. Note that if the width of a feature in a model was smaller than the temporal resolution in the data, we averaged the model over several steps smaller than the width of the feature. The best-fit model contains a constant which describes the non-flaring intensity, two Lorentzians which describe the leading edge and falling edges of the pre-periastron (PP) flare, and a third Lorentzian that describes a near-apastron (NA) flare. Table 1 lists the properties of these modeled components.

The NA flare is very significant:  $\chi^2$  per degree of freedom,  $\chi^2_{d.o.f.}$ , is reduced from 5.5 to 1.0 with the inclusion of this component; it also occurs with similar significance in both the first and second halves of the data. A Gaussian fit to the NA flare is not ruled out:  $\chi^2_{d.o.f.}$  increases from 1.0 to 1.1.

The PP flare is significantly asymmetric. Neither a single Gaussian ( $\chi^2_{d.o.f.} = 4.5$ ) nor a single Lorentzian component ( $\chi^2_{d.o.f.} = 5.1$ ) fits. The rise is three times slower than the fall (Table 1). A Lorentzian component is a somewhat better description of the rise since a Gaussian rise gives  $\chi^2_{d.o.f.} = 1.6$ . A Gaussian fall is not ruled out. We can not determine a lower limit for the width of the fall due to the effective temporal resolution of the data.

The phase of the PP flare peak is determined by the peak in the falling component which is more intense than the rising component. In Table 1 the central phase measurements of the components are in terms of the orbital phase using the Sato et al. elements. The measured PP peak phase is consistent with the result of Sato et al.,  $0.966 \pm 0.007$ , and is about 130 orbital cycles later.

### 3.3 GX301-2 Pulse Period

X-ray pulsations are evident in the *ASCA* data. A narrow peak in the fast-Fourier transform of the data corresponds to a barycentric period of  $675.8 \pm 0.1$  s after corrections for the GX301 -2 orbital period. This value and the  $1-\sigma$  error were calculated by folding the data over the period, fitting a template to a narrow feature in the average pulse, and determining the phase of that narrow feature as a function of time in pulses across the *ASCA* data set. The simultaneous *BATSE* data gives the same value for the period (Koh 1995). Figure 6 shows the time history of the GX301 -2 pulse (Nagase 1989; Alekandrovich et al. 1994a,b; Lutovinov et al. 1994) with the *ASCA* point added, the lowest value observed to date. We also did a linear fit to the spin-up region that is shown as a straight line in the figure. The spin-up is  $-8.3 \times 10^{-6}$  s s<sup>-1</sup>.

### 3.4 GX301-2 Pulse-Phase Averaged Spectrum

The phase-averaged *GIS2* spectrum is shown in Figure 7 together with the “simultaneous” *BATSE* data, where “simultaneous” means taken over the same day with different operational data gaps. The spectrum is fit by a power law model with low energy absorption, a narrow iron emission line, an iron absorption edge, and a high-energy cutoff. The low energy absorption is not well-determined herein because we do not extend our analysis below  $\sim 4$  keV because of the complicating nature of a soft excess (but see Saraswat et al, 1995). For the absorption we use standard elemental abundances relative to hydrogen except for iron for which we separately fit an absorption edge near 7 keV. We obtain a  $\chi^2 = 124$  for 133 degrees of freedom, Table 3 lists the parameters derived from this spectrum where the parameter limits are given for 90% confidence. For the case of the iron line features near 6-7 keV we used the values derived from the higher resolution SIS detectors.

Many pulsar spectra exhibit high energy cutoffs with cutoff energies,  $E_c$ , above which the spectrum falls exponentially with a folding energy,  $E_f$  (e.g. White et al. 1983). Leahy & Matsuoka (1990) found  $E_c \approx 18$  keV and  $E_f \approx 10$  keV in GX301-2. Because of the gap in our spectral coverage between 10 and 20 keV and our lack of sensitivity above 60 keV we have chosen to keep  $E_f = 10$  keV fixed in our model--its best-fit value. This results in  $E_c = 26 \pm 7$  keV, roughly consistent with the previous results. We also attempted to fit a model like that described in Makishima & Mihara (1992) for a cyclotron feature near 40 keV. The data do not require such a feature; its inclusion leads to an increase in  $\chi^2$ .

We measured the *SISO/ASCA* iron line energy to be  $6.41 \pm 0.02$  keV, the energy for neutral iron or with an ionization state no higher than Fe XVIII. The line is narrow,  $43 \text{ eV} < \text{width} < 74 \text{ eV}$ . The iron edge energy is at  $7.19 \pm 0.03$  keV. The line energy implies that the iron ionization state is less than XVII, while the edge energy requires an ionization state less than V (Makishima 1986; c.f. Leahy et al. 1989). These are consistent with nearly neutral iron. The strength of the iron absorption edge implies that iron is more abundant relative to hydrogen by about 50% compared to the standard ratio.

### 3.5 GX301-2 Pulse-Phase Spectroscopy

Spectral data were folded over the observed pulse period, divided into five pulse-phase bins, and analyzed with a model of the form described above. There is variability in the continuum spectrum with pulse phase. Figure 8 shows the pulse intensity profile (bottom panel) and the spectral index from the four detectors (upper panels). Table 4 lists the spectral parameters in the different pulse phase bins. We do not detect any variability in the iron line intensity or energy with pulse phase.

## 4. DISCUSSION

### 4.1 The Pulse Period

The *ASCA/BATSE* determination of the GX301-2 pulse period demonstrates that the spin-up that started in 1984 (-day 6000) continues. This is the longest lasting secular spin-up of the known pulsars. According to Ghosh & Lamb (1979) this trend indicates that an accretion disk is now dominating the mass transfer. In contrast, stellar wind domination of the mass transfer caused the stochastic period behavior in the pre-1984 period. It is interesting to note that there has been no long-term change in the X-ray luminosity of GX301-2 despite the change in period behavior. Since at least 1973 (Forman et al. 1978) the X-ray intensity has been near  $1\text{-}2 \times 10^{-9} \text{ erg cm}^{-2} \text{ s}^{-1}$ , depending on the energy range of the detectors.

The spin-up corresponds to a  $dP/dt P^{-1} = -3.9 \times 10^{-3} \text{ yr}^{-1}$ . From Ghosh & Lamb  $dP/dt P^{-1} \sim 7 \times 10^{-5} P L_{37}^{67}$  for a "slow rotator" where  $L_{37}$  is the x-ray luminosity in units of  $10^{37} \text{ erg s}^{-1}$ . In this observation the 4-60 keV intensity is  $1.9 \times 10^{-9} \text{ erg cm}^{-2} \text{ s}^{-1}$  which corresponds to  $7.8 \times 10^{35} \text{ erg s}^{-1}$  at a distance of 1.8 kpc (Nagase 1989). Inserting this value into the equation,  $dP/dt P^{-1} = -5.3 \times 10^{-3} \text{ yr}^{-1}$ , close to the measured value. In a recent report (Kaper et al. 1995) WRAY 977 is reclassified as a B I Ia+ hypergiant and its distance is estimated to be 5.3 kpc. This would increase the X-ray luminosity to  $6.8 \times 10^{36} \text{ erg s}^{-1}$  and  $dP/dt P^{-1} = -3.4 \times 10^{-2} \text{ yr}^{-1}$ , a value that is 10 times larger than the observed.

## 4.2 The Orbital Light Curve

The *BATSE* data allow us to put the *ASCA* observation in the context of the long-term GX301 -2 behavior. In particular the *ASCA* observation occurred during a non-remarkable time in the non-flaring portion of the light curve.

We use the *BATSE* data to refine models of the binary system. Since these data are for  $E > 20$  keV there are no complicating effects of low energy absorption. The folded curve over orbital period (Figure 5a) shows the unattenuated source, and thus is closely linked with the mass transfer.

There are two new features in these data: the discovery of a periodic NA flare and the asymmetry of the PP flare. The periodic flares are difficult to explain with isotropic stellar wind accretion alone. Both the flares and the PP asymmetry, however, might be explained by the interaction of GX301 -2 with an equatorially-enhanced stellar wind (Waters et al. 1988) or a circumstellar disk around WRA 977. Disks are believed to form in X-ray binary pulsar systems containing Be stars (e.g. Coe et al. 1993). While WRA 977 is not a Be star the GX301 -2 system shares properties with Be star systems (Iye and Kodaira 1985, Apparao 1993, Kaper et al. 1995). It also exhibits  $12 \mu\text{m}$  emission, a disk indicator, at about 1/5 the level seen in the Be star X Per (Smith et al. 1990). We therefore compare our results to Be star disk models (e.g. Bjorkman and Cassinelli 1993).

In our model the two flares which are separated by about 0.5 phase occur when the misaligned pulsar orbital plane crosses the equatorial disk of the primary (e.g. Kelley et al. 1983). We can empirically determine some parameters of this putative disk by examining the flares. The flares occur near radii  $R_p = 2.1R_s$  and  $R_a = 6.0R_s$  for periastron and apastron, respectively, where  $R_s = 43 R_\odot$  (Parkes et al. 1980) is the stellar radius.

In this model the temporal widths of the flares are equal to the effective thicknesses of the disk at the flare radii divided by the neutron star velocities,  $v \sin i$ , where  $i$  is the inclination angle between the orbital and disk planes. The effective thicknesses are those for which a significantly larger amount of material is captured by GX301 -2 than during the steady-state non-flaring X-ray phases. The latter arises when the neutron star is in the nearly isotropic regions of the stellar wind. From Table 2 this yields thicknesses of  $2.2 \sin i R_s$  and  $0.7 \sin i R_s$  for periastron and apastron, respectively. For small angles, e.g.  $i = 10^\circ$  these thicknesses become  $0.4 R_s$  and  $0.1 R_s$ . The apastron value is consistent with a disk opening angle of  $0^\circ.5$ , while the periastron region is considerably larger than a narrow disk.

The relatively gradual rise in the PP flare occurs with a width of 1.64 days. This occurs as GX301 -2 approaches periastron and captures additional material from the primary disk. When GX301 -2 exits from the primary disk the mass transfer rapidly shuts off with a width of 0.50 days. This asymmetry in the mass transfer may occur via an asymmetrically shaped transition region like the curved gas stream discussed by Haberl (1991). The circumstellar disk can also introduce an asymmetry if the disk velocity differs from that of GX301-2. For example, if GX301-2 overtakes slower disk material during ingress and leaves it behind during egress a flare could result that rises less rapidly than it falls. Alternatively, the pulsar accretion disk could mediate the transfer and make it asymmetric by virtue of the well-defined direction of the spin. Near apastron we are unable to measure any asymmetry in the flare due to the lower statistical quality of the light curve.

The flare intensities are proportional to the mass transfer rates at the flare radii. The ratio of the PP to NA flare intensities is  $\sim 5$ . This is a surprisingly low ratio considering the eccentricity of

the orbit. Bjorkman & Cassinelli (1993) find a density ratio of  $\sim 100$  for disk material and  $\sim 10$  for wind material at this periastron to apastron ratio. If these density ratios are correct then the material capture cross section onto the neutron star favors accretion at apastron.

We can pull together some of the observed phenomena in the following way. We suggest that the NA flare has appeared in coincidence with the secular spin-up behavior. This points to a change in the system--the growth or enhancement of a circumstellar disk--that both defines a plane where both sets of flares occur and steadily adds angular momentum to the neutron star. During the pre-1984 era of period behavior this disk was so small that only the PP flare occurred, i.e. the disk did not significantly extend to the apastron radius, and the angular momentum transfer was stochastic.

#### 4.2 *The Pulse-Phase-Averaged Broadband X-ray Spectrum*

The pulse-phase-averaged 4-60 keV spectrum measured simultaneously with ASCA and BATSE is similar to that seen previously (Leahy & Matsuoka 1990; Aleksandrovich et al. 1994a). Below 4 keV the presence of unrelated sources 3' and 8' from GX301 -2 indicates that at least some of the previously detected soft excess did not originate in GX301 -2 ( e.g. Haberl 1991; but see Saraswat et al. 1995). White & Swank (1984) discuss other properties of the soft component that suggest it originates in a source other than GX301 -2.

The iron line and edge energies are consistent in these observations with neutral or nearly neutral iron. The line is the result of fluorescence in circumstellar material that is considerably cooler than the X-ray emission region (e.g. Kallman & McCray 1982). The same material when directly in the line of sight absorbs X-rays and forms the iron absorption edge. The depth of the edge that we detect implies that iron is over-abundant relative to hydrogen by about 50% when compared to cosmic abundances. We do not observe the inconsistent ionization states between the line and edge that Leahy et al. (1989) saw.

#### 4.3 *Spectral Variability with Pulse Phase*

Our results confirm those of Leahy & Matsuoka (1990) in that the continuum hardens in the interpulse region. The hardest spectrum is in our second phase bin. Other pulsars (e.g. Her X-1) also show a harder spectrum in the "interpulse" region. This has been associated with a view deeper into the polar cap along magnetic field lines (Pravdo et al. 1977, Harding et al. 1984).

There was no significant variability in the iron line intensity with pulse phase. This contrasts with Leahy & Matsuoka (1990) in which they saw variability during the PP flare. We checked for but did not find iron line energy variability with pulse phase.

### 5. CONCLUSIONS

These observations with ASCA and BATSE/GRO lead to the following conclusions:

1. The X-ray light curve with orbital phase shows that GX301 -2 interacts twice per orbit with an equatorially-enhanced stellar wind or a circumstellar disk around WRAY 977. This disk may also provide a steady source of angular momentum to the neutron star causing the secular spin-up.
2. At least two soft X-ray sources are located within 8' of GX301 -2. and probably contributed to previous observations of a soft X-ray excess.
3. The iron line and edge energies are consistent with a single ionization state less than Fe V. There is no apparent iron line intensity or energy variation with pulse phase in these data.

| “ ’ ”

We thank S. Ryan for providing the GXS optical spectrum and useful comments on the analysis thereof We also thank D. Koh and D. Chakrabaty for sharing the BATSE pulse period data prior to publication. This research has made use of the *Simbad* database, operated at CDS, Strasbourg, France.

## REFERENCES

- Aleksandrovich, N. L. et al. 1994a, COSPAR in Hamburg  
Aleksandrovich, N.L. et al. 1994b, *Astr. Letters*, 20, 565  
Apparao, K. M. V. 1994, *A Ap*, 291, 775  
Bjorkman, J. E. & Cassinelli, J. P. 1993, *Ap J.*, 409,429  
Coe, M. J. et al. 1993, *A Ap Suppl.*, 97,245  
Fishman, G. J. et al. 1989, in *Proc. GRO Science Workshop*, ed. W. N. Johnson (Greenbelt: NASA/GSFC), 2-39  
Forman, W. et al. 1978, *Ap J Suppl*, 38, 357  
Ghosh, P. & Lamb, F. K. 1979, *Ap J*, 234, 296  
*Guide Star Catalog*, 1989 (Baltimore: Space Telescope Science Institute)  
Haberl, F. 1991, *Ap J*, 376, 245  
Harding, A. K. et al. 1984, *Ap J*, 278, 369  
Iye, M. & Kodaira, K. 1985, *PASP*, 97, 1186  
Kallman, T. & McCray, R. 1982, *Ap J Suppl*, 50, 263  
Kelley, R. L. et al. 1983, *Ap J*, 274,765  
Koh, D. 1995, private communication  
Leahy, D. A. 1991, *MN R A S*, 250, 310  
Leahy, D. A. et al. 1989, *M N R A S*, 237,269  
Leahy, D. A. & Matsuoka, M. 1990, *Ap J*, 355, 627  
Lutovinov, A. A. et al. 1994, *Astr. Letters*, 20, 538  
Makishima, K. 1986, *Lecture Notes in Phys.*, 266, 249  
Makishima, K. & Mihara, T. 1992, in *Frontiers of X-ray Astronomy*, p. 23 (Universal Academy Press Inc.)  
Marraco, H.G. & Orsatti, A.M. 1982, *Rev Mex A Ap*, 5, 183  
Nagase, F. 1989, *P A S J*, 41, 1  
Parkes et al. 1980, *MNRAS*, 191, 547  
Pravdo, S. H. et al. 1977, *Ap J*, 216, L23  
Ricker, G. R. et al. 1973, *Ap J*, 184, 237  
Robinson, R. D. 1990, *Ap J Suppl*, 74, 891  
Saraswat, P. et al. 1995, preprint  
Sate, N. et al. 1986, *Ap J*, 304,241  
Smith, H. A. et al. 1990, *A J*, 99, 273  
Stevens, I. R. 1988, *M N R AS*, 232, 199  
Swank, J. H. et al. 1976, *Ap J (Letters)*, 209, L57  
Tunics, Y. et al. 1994, *P A S J*, 46, L37  
Waters, L. B. F. M. et al. 1988, *A Ap*, 198,200  
White, N. E. et al. 1976, *Ap J*, 209, L119  
White, N. E. et al. 1983, *Ap J*, 270, 711  
White, N. E. & Swank, J. H. 1984, *Ap J*, 287, 856

Table 1. GXS Optical Lines

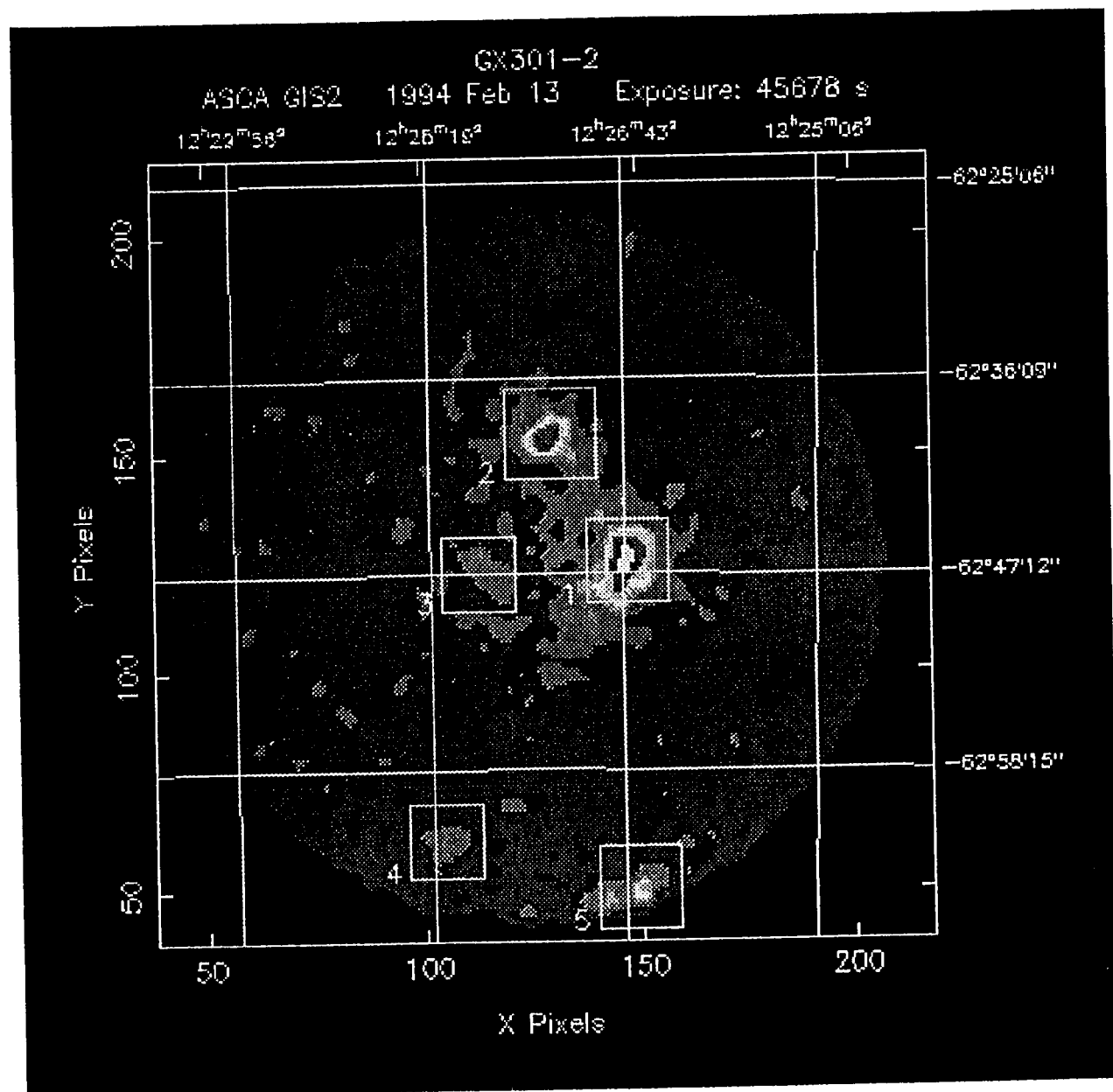
Line	Equivalent Width (Å)
Ca II K	7.30±0.08
Ca II H	4.66±0.08
H $\epsilon$	2.02±0.04

Table 2. GX 301-2 Orbital Light Curve

Component	Intensity (photon s <sup>-1</sup> )	Central Phase	Width (Days)
Constant	0.023±0.005	...	...
Pre-periastron rise	0.14 (+0.05,-0.03)	0.923±0.016	1.64 (+0.37,-0.62)
Pre-periastron fall	0.33 (+.. -0.08)	0.970±0.003	0.50 (+0.29,-...)
Near-apastron	0.053± (+0.015,-0.022)	0.473±0.013	1.91 (+1.33,-0.91)

Table 3. GX301-2 Average Spectrum from GIS and BATSE

Parameter	Value
Normalization	0.107(+0.45,-0.32)
Photon index	1.28±0.16
$N_H$	5.3+03x 10 <sup>22</sup> cm <sup>-2</sup>
Fe line energy	6.41±0.02 keV
Fe line e.w.	227±21 eV
Fe edge energy	7.19±0.03 keV
Fe edge $\tau$	0.76±0.05
Cutoff energy	26±7 keV
Cutoff folding energy	10 keV (fixed)



GX      tak    th

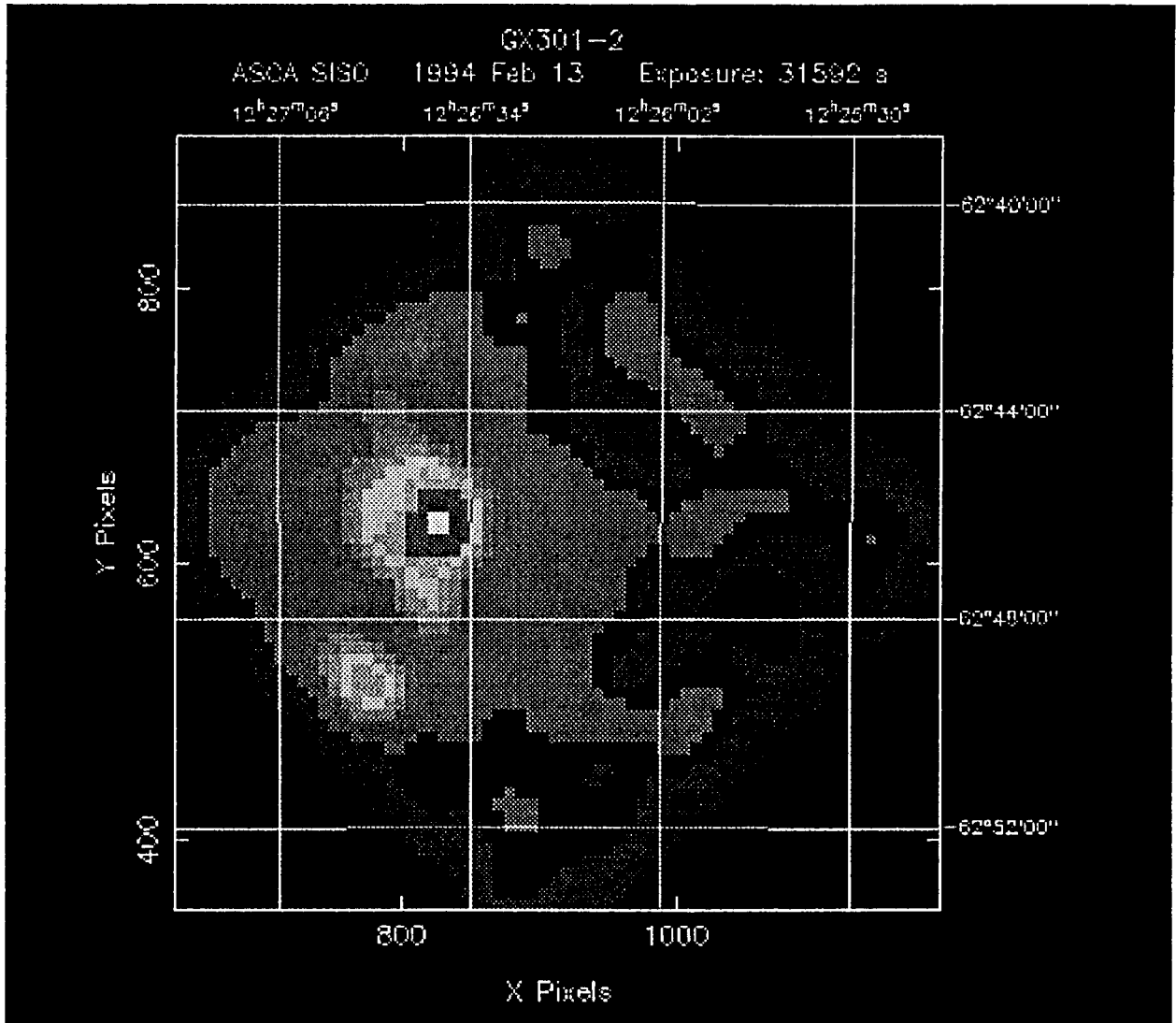


Figure 1b. GX301-2 field taken with *SIS0/ASCA*.

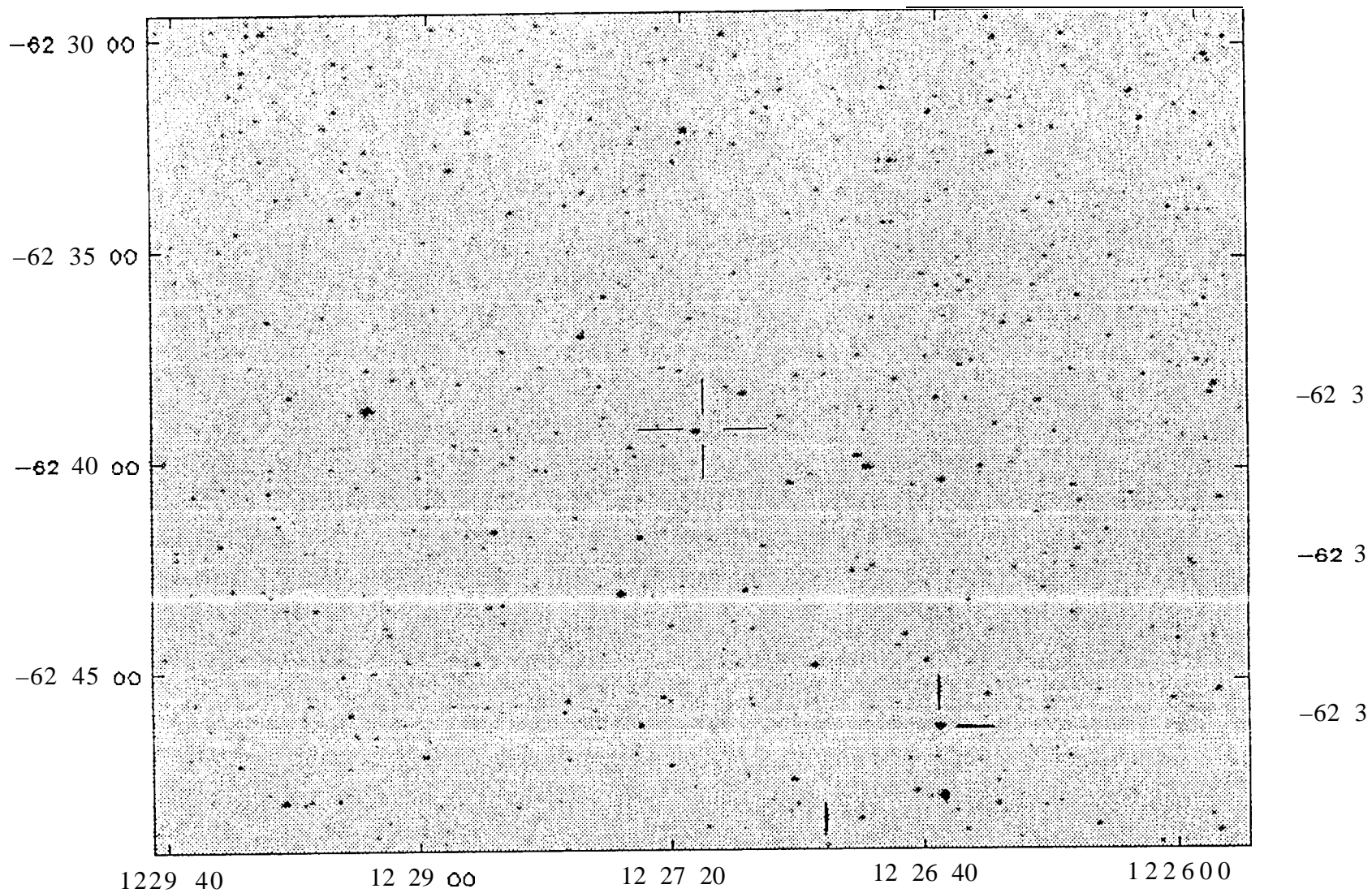


Figure 2. AX1227-6239 (GXS) finding chart. GX301-2 is to the southwest. Near the edge of the frame to the southeast of GX301-2 is a candidate star for AX1226-6249 (SXS).

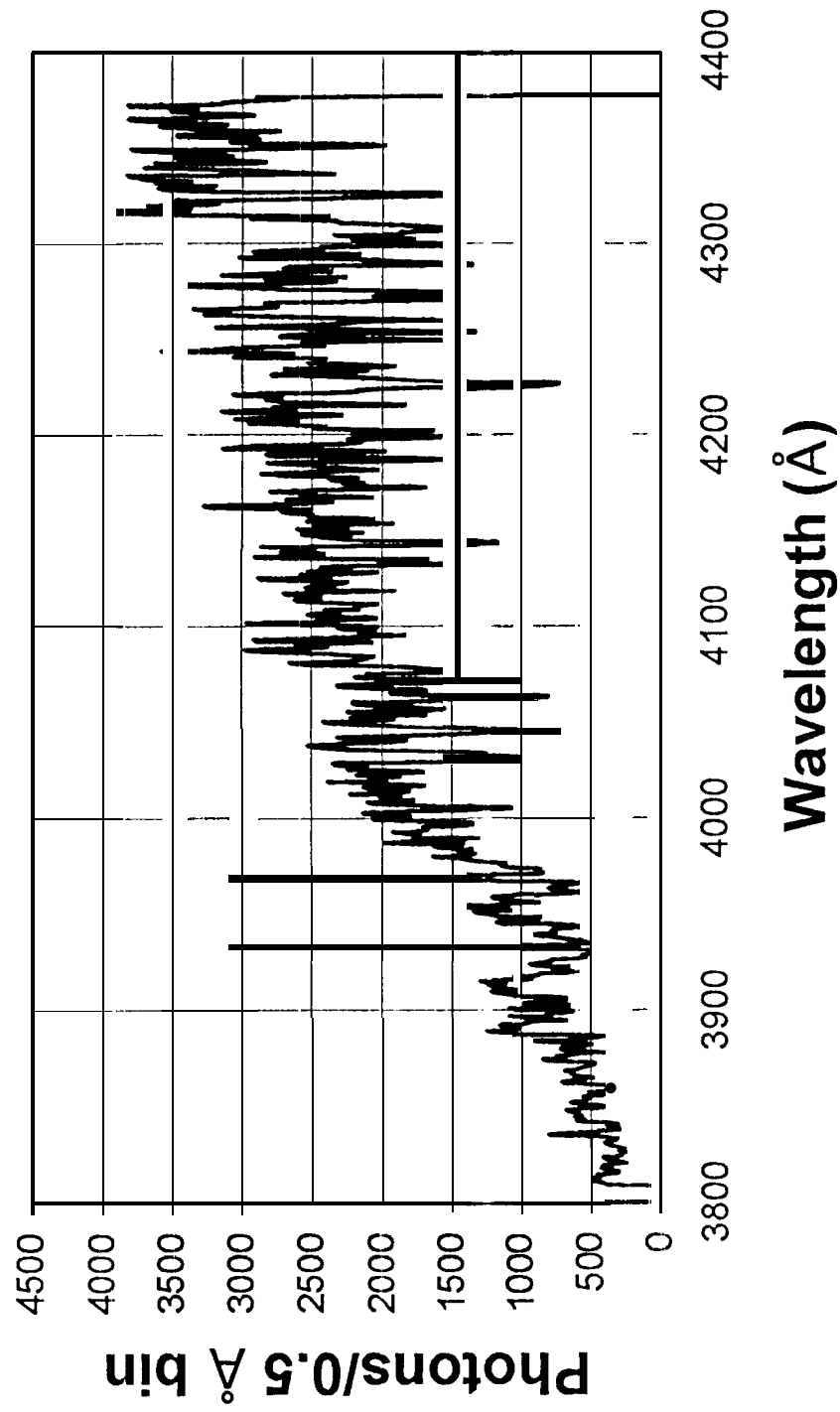


Figure 3. Blue spectrum of AX1227-6239 (GXS) obtained with the Australian National University's 2.3 m telescope at Spring using the Double Beam Spectrograph with the 1200 l/mm grating blazed at 4100Å.

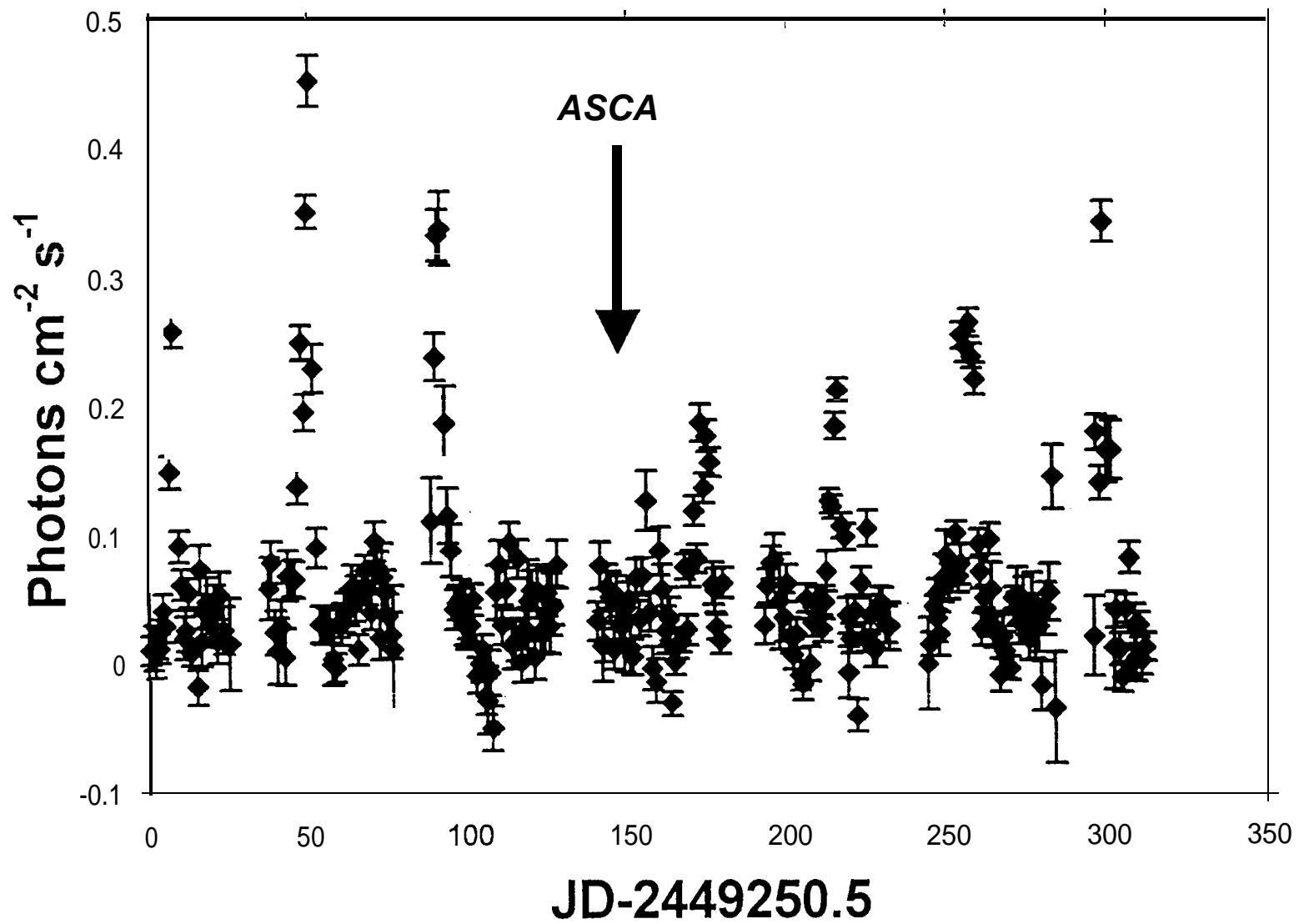


Figure 4. GX301-2 *BATSE/GRO* 20-60 keV light curve.

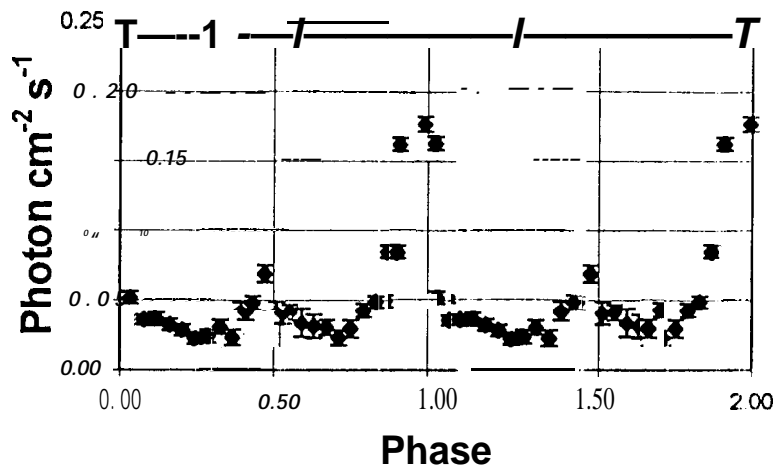


Figure 5a. GX301 -2 *BATSE* light curve folded over the orbital or flare period (two cycles).

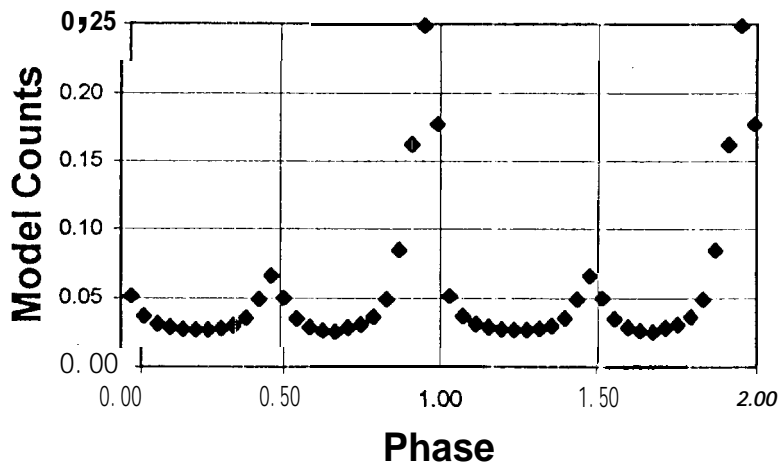


Figure 5b. Model of folded light curve.

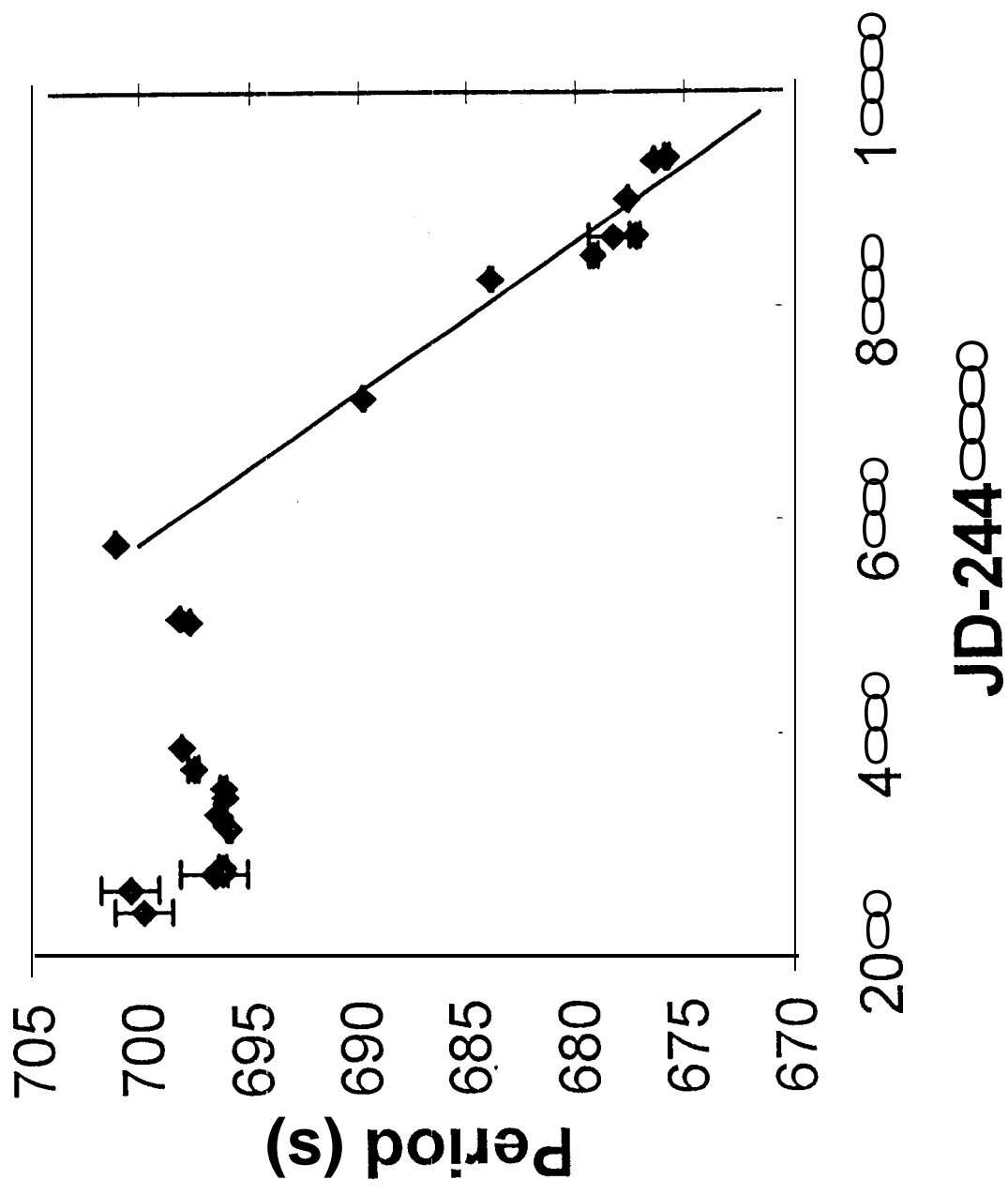


Figure 6. GX301-2 pulse period time history. The line is the linear fit to the spin-up and corresponds to  $-8.26 \times 10^{-8} \text{ s}^{-1}$ .

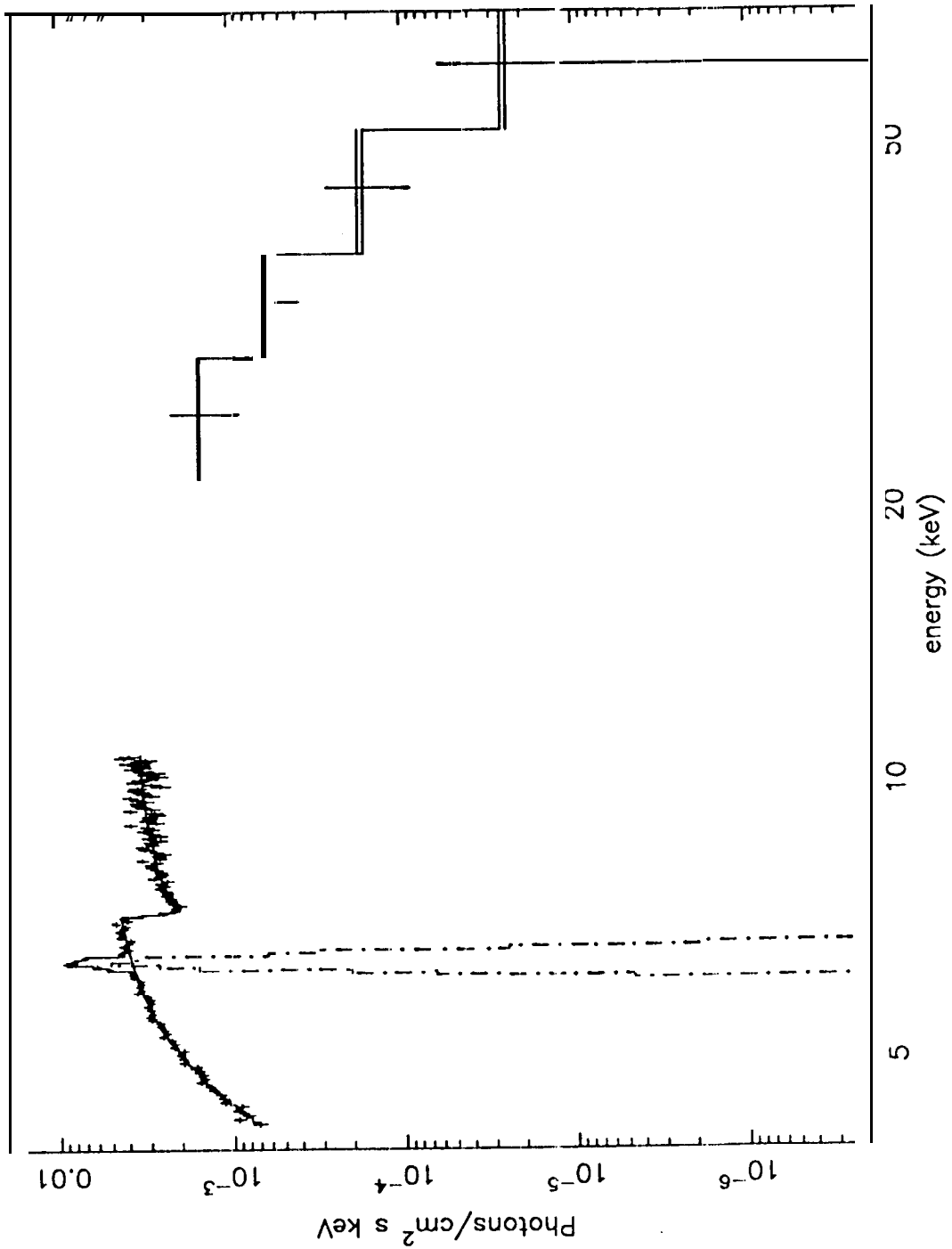


Figure 7. GX301-2 average spectrum with GIS2/ASCA and BATSE/GRO.

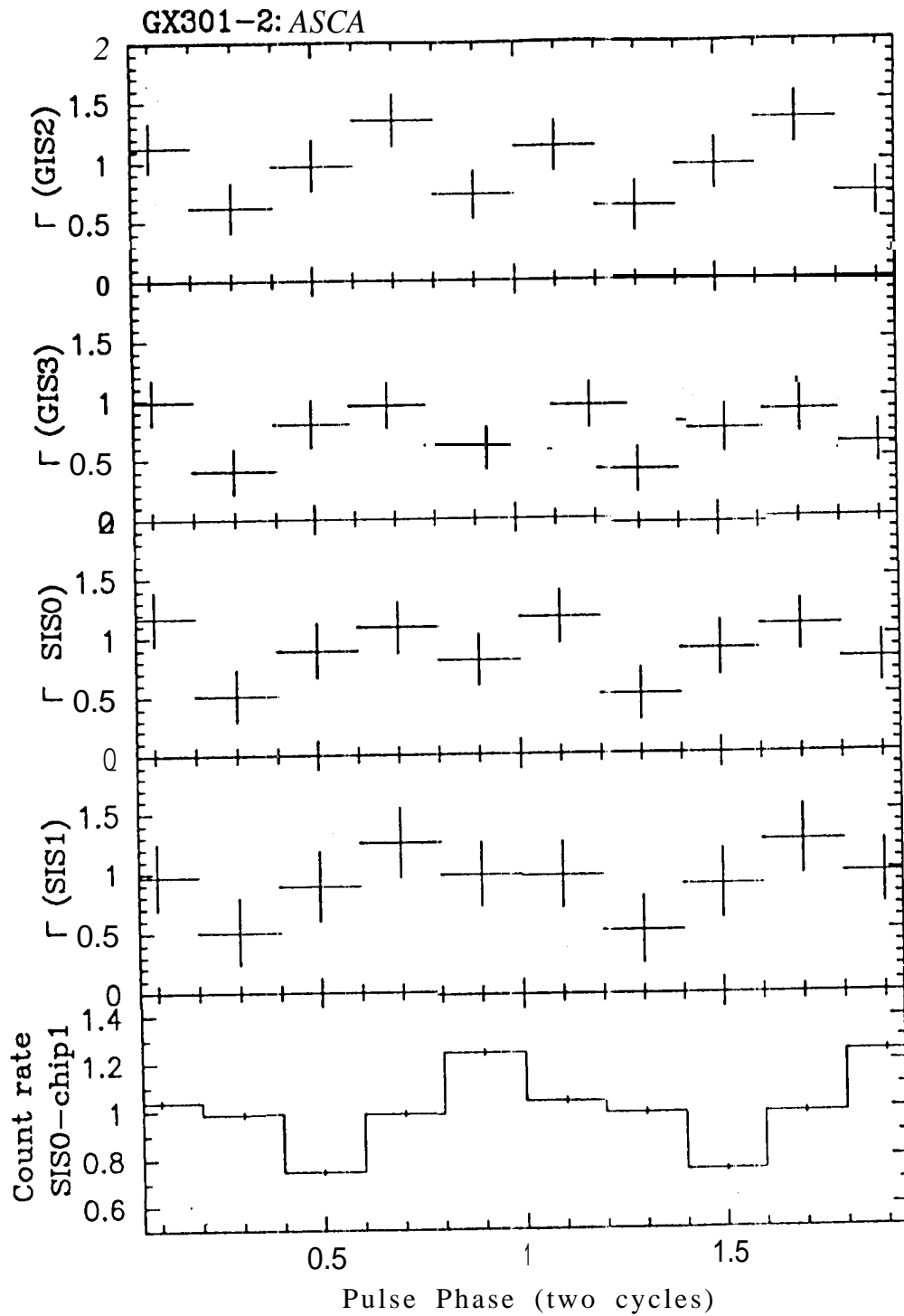


Figure 8. Pulse-phase variability of the GX301-2 spectral index seen with ASCA. The top four panels show the spectral index with pulse phase for the four detectors. The bottom panel shows the pulse intensity profile from the *SISO* detector.